Acta Materialia 207 (2021) 116664

Contents lists available at ScienceDirect

Acta Materialia

journal homepage: www.elsevier.com/locate/actamat

Combinatorial structural-analytical models for the prediction of the mechanical behaviour of isotropic porous pure metals

L. Bolzoni*, J.K. Carson, F. Yang

School of Engineering, The University of Waikato, Hamilton 3240, New Zealand

ARTICLE INFO

Article history:
Received 3 November 2020
Revised 10 January 2021
Accepted 16 January 2021
Available online 20 January 2021

Keywords:
Porous materials
Mechanical behaviour
Structural-analytical model
Modelling
Sintering

ABSTRACT

This work provides insight on the prediction of the mechanical behaviour of isotropic porous pure metals using empirical and structural-analytical models and proposes two new combinatorial structural-analytical models for the estimation of the mechanical properties. Porous metals such as foams are advanced engineering materials and therefore the prediction of their properties for their optimisation is beneficial. Nevertheless, the estimation of their mechanical behaviour generally relies on semi-empirical models, which are limited to specific materials (i.e. type of metal + type of internal structure + individual property) and for which empirical constants need to be determined. Among the available structural-analytical models, which were developed to estimate mathematically equivalent thermophysical properties, the Symmetric and Interconnected Skeleton Structural (SISS) model gives the best prediction over a broad range of volume fraction of pores (i.e. 0.4–1.0) but always significantly overestimates the elongation to failure. This study presents the derivation of new combinatorial structural-analytical models that are able to rapidly and accurately predict the Young modulus plus ultimate tensile strength and the elongation to failure, respectively, across the entire range of volume fraction of pores. These models have physical bases, are not time- and computing-intensive (thus rapid and low cost), and have reasonable accuracy for materials whose microstructure is uncertain.

1. Introduction

The mixture of two or more existing materials in a chosen architecture to superimpose their properties is termed as the creation of hybrid materials. Among these hybrid materials, porous materials and especially metallic foams are considered advanced materials. This is because they generally have controlled meso- and micro-pores distributed within the microstructure, which gives rise to unique combinations of properties. This makes them attractive for a great variety of engineering applications [1,2]. Such applications include: (1) lightweight sandwich panels (lighter and potentially stronger/stiffer than conventional honeycomb structures) [3]; (2) impact energy absorption devices (due to the ability to undergo significant amount of deformation, as high as 70%, at almost constant applied load) [4]; (3) heat sinks (due to their high thermal conductivity combined with high surface area) [5]; and (4) artificial bone replacements (due to the ability to match the Young modulus of human bones) [6]. This is possible because the microstructure of porous materials is made up of interconnected struts.

Porous metals can be produced using a wide range of manufacturing techniques including melt processing routes, which generally rely on the addition of a blowing agent into a molten metal (e.g. TiH_2 in Al) and are preferred for low melting point metals [7], and solid state methods. Among powder metallurgy solid state processes there are partial sintering [8], sintering of hollow spheres [9], sintering of materials with space holders [10], and sintering of materials with entrapped and expanding gas [11]. Partial sintering is the easiest manufacturing method where the desired level of volume fraction of pores is commonly obtained via compaction at low pressures combined with low-temperature sintering [12,13]. Specifically, sintering is limited to the early stages of neck formation between individual powder particles as to be able to retain a significant amount of residual pores [14].

The specific thermal, mechanical, acoustic and electrical properties of porous materials are significantly affected by the combination of manufacturing process used (i.e. type of method, processing parameters, etc.) and the physical structure obtained. This includes parameters like cell wall thickness and relative density (or volume fraction of pores). Consequently, for optimising the design of

* Corresponding author.
E-mail address: leandro@waikato.ac.nz (L. Bolzoni).

https://doi.org/10.1016/j.actamat.2021.116664

Nomenclature

a	Length of the outer cross-section of struts
b	Length of the inner cross-section of struts
C^*	Empirical parameter of the Gibson and Ashby model
CCM	Co-Continuous Model
E	Young modulus
El	Elongation to failure
EMT	Effective Medium Theory
HDH	Hydride-dehydride process
k	Constant of the percolation theory
ME1	Maxwell-Eucken 1 model
ME2	Maxwell-Eucken 2 model
n^*	Exponent of the Gibson and Ashby model
N	Number of phases
PM	Parallel Model
SISS	Symmetric and Interconnected Skeleton Structural model
SM	Series Model
t	Fitting exponent of the percolation theory
UTS	Ultimate tensile strength
v	Volume fraction of a phase

Greek

ρ	Density of the material
ψ	Generic property of a porous material (e.g. thermal conductivity, E, etc.)
ϕ	Structure composition factor

Subscripts

1, 2	Phases composing the porous material
AM1	Structural-analytical model one
AM2	Structural-analytical model two
c	Critical concentration (threshold) of the percolation theory
f	Fluid phase
h	Hollow struts
i	i^{th} phase
s	Solid phase

customised porous materials, the prediction of physical and mechanical properties is required.

The estimation of physical properties like thermal conductivity and electrical resistivity is commonly done via modelling. Many of the proposed models are either purely empirical or are theoretically based but highly specific to a given material. Structural-analytical models are also available (see Appendix for more details) but, generally, fundamental structural-analytical models such as the Maxwell-Eucken (ME) model and the effective media theory (EMT) [15] cannot accurately predict the effective properties across the full range of volume fraction of pores. Furthermore, other structural models such as the Gibson and Ashby and the hexagonal strut structure [16] generally need empirical parameters for accurate predictions.

Regarding the prediction of the mechanical behaviour of porous materials in general, and the tensile properties in particular, either numerical simulations or semi-empirical models need to be used. The former are rigorous time- and computing-intensive simulations done using the finite difference or the finite element methods in order to describe the physical structure accurately. Empirical or semi-empirical models are obtained by modifying fundamental models using a fitting parameter and thus they have limited applicability. An example of the latter is the Gibson and Ashby model [17] (see Appendix for more details) which includes an empirical parameter C^* and an exponential term n^*. C^* is related to the physical structure of the material and, in the case of the Young modulus, $C^* = 0.98$ for open cell foams and $C^* = 0.32$ for closed cell foams [2]. In the case of the Young modulus, $n^* = 2$ for open cell foams and $n^* = 1$ for closed cell foams [2]. A typical example of the need of adjusting the empirical parameters to fit the experimental data can be found in the review of Shbeh and Goodall (Fig. 12 and Fig. 13 in [14]) or the work of Esen and Bor [18] ($C^* = 1.598$ and $n^* = 4.72$ for titanium foams).

From literature about the estimation of properties such as electrical resistivity, thermal conductivity, and magnetic permeability of porous materials, structural-analytical models are generally preferred over numerical simulation due to their physical basis, rapid and low cost of calculation, and reasonable accuracy even when the microstructure is uncertain [19]. Although not previously attempted, these structural-analytical models could, due to mathematical analogy [20], potentially be developed and implemented to predict the mechanical behaviour of porous materials. Therefore, the aim of this work is to verify the applicability and accuracy of existing structural-analytical models. For that, models' predictions are compared to experimental data originated from different isotropic pure metals either purposely made to quantify the accuracy of the prediction, or available in literature. The work is complemented with the analysis of the data through empirical models to prove their applicability. Finally, new combinatorial structural-analytical models able to successfully predict the mechanical behaviour (viz. E, UTS and El) of porous materials over the whole range of volume fraction of pores are proposed/derived and their accuracy discussed.

2. Preparation and characterisation of the isotropic porous pure metal samples

A hydride-dehydride (HDH) pure Ti powder with particle size lower than 75 μm (oxygen content 0.23 wt.%), a pure Fe powder with particle size lower than 10 μm, and NaCl powder with particle size lower than 800 μm were the starting materials for the production of the porous samples through the space holder technique. It is worth mentioning that the space holder technique and NaCl were chosen for the sake of simplicity. As can be seen from Fig. 1, which presents micrographs (SEM - Hitachi S4700 and OM - Olympus BX60) showing the morphology of the starting materials, the HDH Ti powder has angular morphology, Fe has spherical morphology, and NaCl has angular morphology. These powder were selected because they are readily available, can be successfully sintered and there is current literature available to guide the selection of their sintering conditions [8,10,21,22].

The correct amount of metal and NaCl powders were mixed to produce porous metals with targeted 0.3 to 0.7 of volume fraction of pores. It is worth mentioning that the size of the NaCl particles added to either Ti or Fe were different as NaCl was sieved through the 40 mesh (i.e. 400 μm) for Ti and through the 60 mesh (i.e. 250 μm) for Fe as these metallic powders have different particle sizes. The powder blends were cold uniaxially compacted at the minimum pressure that guaranteed shaping and ejection without fracture of the 40 mm diameter cylindrical samples. Sintering of the shaped powder blends was done using a two-stage sintering cycle of 800 °C for 2 h plus 1100 °C for 2 h using a heating rate of 10 °C/min. For the removal of the NaCl space holder, the sintered samples were placed into an ultrasonic water bath for 12 h, and finally dried at 80 °C for 4 h. The sintering and NaCl removal parameters were chosen on the basis of current literature on the production of porous materials via sintering [8,10,21,22].

Characterisation of the porous samples revealed that the production of porous Ti and Fe samples through the space holder method [10] using vacuum sintering permits effective creation of porous metals. Specifically, porous materials with volumetric frac-

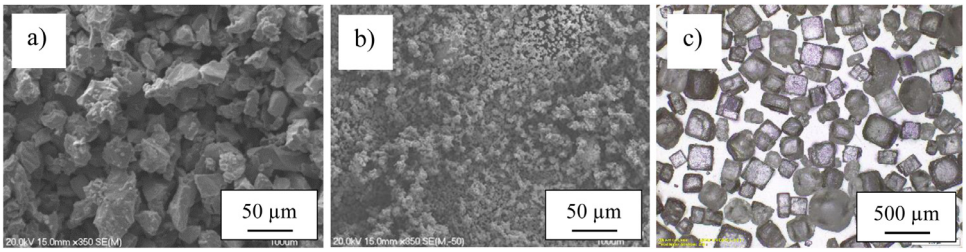

Fig. 1. SEM/OM micrographs of the morphology of the starting powders: a) HDH Ti, b) Fe, and c) NaCl.

Table 1
Details of the sintered materials including actual volume fraction of pores and relative density.

Material	Sample	% of NaCl	Actual volume fraction of pores	Relative density [%]
Ti	Ti - S1	30	0.443	55.7 ± 0.1
	Ti - S2	50	0.568	43.2 ± 0.5
	Ti - S3	70	0.711	28.9 ± 0.1
Fe	Fe - S1	30	0.381	61.9 ± 0.4
	Fe - S2	50	0.579	42.1 ± 0.1
	Fe - S3	70	0.756	24.4 ± 0.2

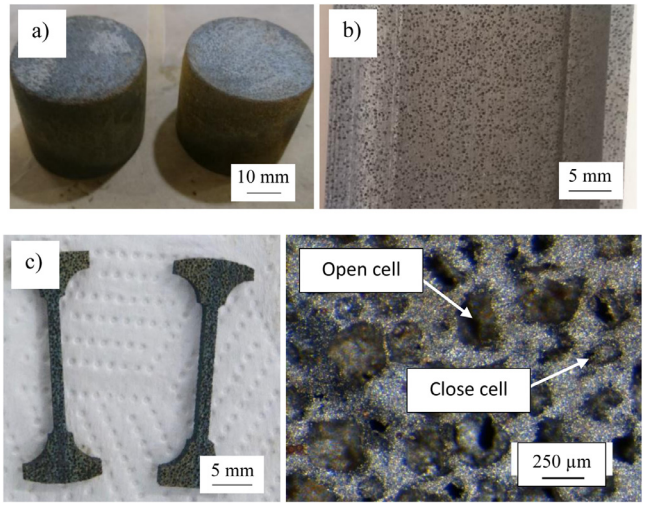

Fig. 2. Representative images of the isotropic porous pure metal sintered samples: a) digital image of the cylindrical samples (S1), b) digital image of the vertical cross section of the porous samples (S2), c) digital image of the profile of the tensile samples (S2), and d) optical micrograph of the horizontal cross section of the isotropic porous pure metal samples (S3).

tion of pores between 0.38 and 0.75 (Table 1) and two types of pores were produced. However, the actual volume fraction of pores present in the sintered materials differed from the targeted value. A progressively lower amount of volume fraction of pores than the one targeted is found as the relative density of the sintered samples increases. This is because the lower the amount of NaCl, the greater the coordination number of the metallic powder particles. Consequently, the higher the amount of necking and densification occurred during sintering, as all materials were sintered under the same conditions.

Fig. 2 shows representative images of the synthesised samples where it can be seen that the materials could successfully be manufactured retaining their cylindrical shape (Fig. 2a). The porous materials have homogeneous distribution of pores along the vertical cross-section (Fig. 2b). Porous dogbone-shaped tensile samples (Fig. 2c) were cut from the cylindrical samples, and the horizontal cross-section of the sintered samples is composed of stochastically distributed pores (Fig. 2d). In particular, the materials have a significant amount of interconnected pores whose size is comparable to that of the NaCl particles used as space holder, and a small amount of closed cells. From the quantitative metallographic study, approximately 50 μm to 400 μm were identified as the average size of the closed and open pores. The majority of the pores are actually macropores left by the dissolution of the place holder but there is a minority of closed cell pores due to the partial sintering of the metallic powder particles.

Dogbone-shaped tensile specimens with rectangular cross section (approx. 2 × 2 mm^2) and gauge length of 20 mm were wire cut from the sintered 40 mm cylindrical samples. The surfaces of the wire cut samples were ground with emery papers to remove the effect of the roughness left by the cutting process and standardise the surface finishing. Tensile tests (Instron 33R4204) were conducted using a strain rate of 5×10^{-3} s^{-1} while the elongation was recorded by means of an external 10 mm mechanical extensometer. The chosen strain rate is one of the most common for tensile testing of metallic materials as per ASTM E8.

The characteristic tensile stress-strain curves of the sintered Ti and Fe porous samples are presented in Fig. 3. Regardless of the actual volume fraction of pores, the Fe samples have a well-defined elasto-plastic tensile behaviour whilst the Ti samples are characterised by a less defined elasto-plastic behaviour, more similar to a pseudo-plastic response. Therefore, the transition from the elastic region to plastic deformation is much more marked for the Fe samples in comparison to the Ti samples. Moreover, from the response to the applied quasi-static load and the average tensile properties (Fig. 3c), the Young modulus (E), the ultimate tensile strength (UTS) and elongation to failure (El) of the porous materials decreases with the volumetric fraction of pores (S3→S1). This is expected as there is less material in the cross-section of the tested samples that is actually withstanding the applied load as the volumetric fraction of pores increases. In terms of absolute values, the Ti samples are generally stronger but less ductile than the Fe samples, as the UTS values are higher and El values are lower. This is due to the combination of the different volumetric fraction of pores of each sample (Table 1) and the intrinsic lattice of each metal as the hcp lattice of Ti has less ability to deform but higher load bearing capability.

3. Accuracy of the estimation of the mechanical behaviour of isotropic porous pure metals

3.1. Semi-empirical models

As mentioned in the introduction, semi-empirical models are commonly used in literature to analyse data but their applicability is generally limited as empirical constants need to be obtained from experimental data. Moreover, the accuracy of a specific empirical model can also be affected by the nature of the data used as it generally works well for a particular set of data (the ones from which it is derived) but does not usually provide an effectively comprehensive prediction. To support these statements,

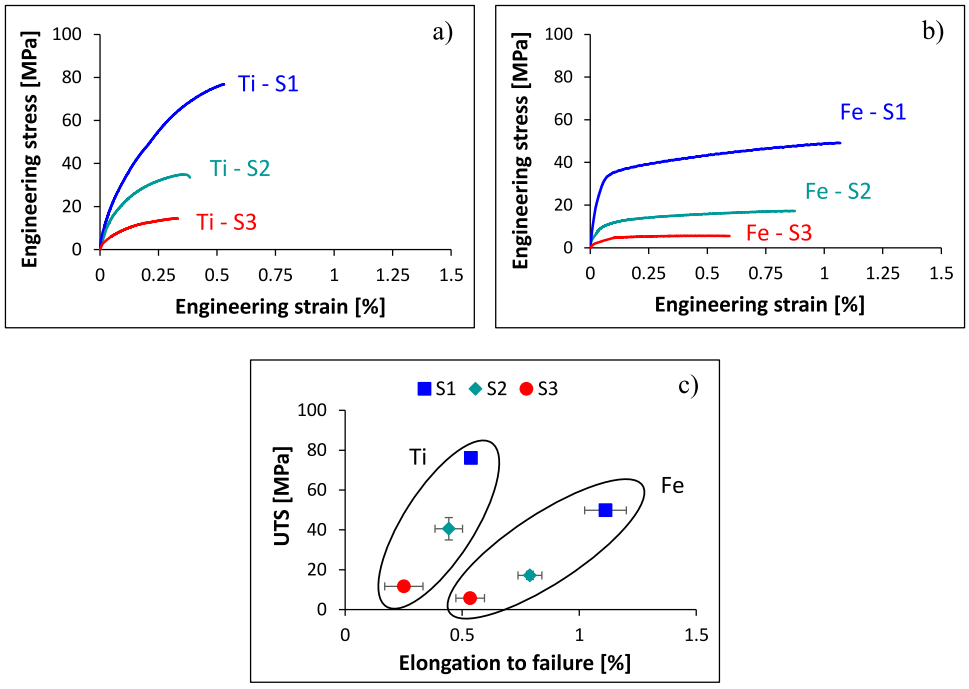

Fig. 3. Results of the tensile testing of the isotropic porous pure metals: a) stress-strain curves of the Ti samples, b) stress-strain curves of the Fe samples, and c) average UTS and elongation to failure values.

Table 2
Values of the empirical constants of the Gibson and Ashby model and of the percolation theory and R^2 values.

Property	C^*	n^*	k	t	R^2	Reference
E_{Ti}	0.786	2.49	–	–	0.9733	Fig. 4a)
	–	–	0.926	1.99	0.9629	Fig. 4c)
UTS_{Ti}	1.095	3.08	–	–	0.9783	Fig. 4a)
	–	–	1.344	2.46	0.9717	Fig. 4c)
El_{Ti}	0.313	2.92	–	–	0.8453	Fig. 4a)
	–	–	0.375	2.31	0.8226	Fig. 4c)
Overall	0.646	2.83	–	–	0.7580	Fig. 4a)
	–	–	0.776	2.25	0.7468	Fig. 4c)
$E_{Ti\text{-}overall}$	0.451	2.01	–	–	0.4859	Fig. 4b)
	–	–	0.432	1.44	0.4420	Fig. 4d)
$E_{Fe\text{-}overall}$	0.903	2.54	–	–	0.9238	Fig. 4b)
	–	–	0.675	1.54	0.9128	Fig. 4d)
$E_{Al\text{-}overall}$	0.315	0.98	–	–	0.3859	Fig. 4b)
	–	–	0.238	0.56	0.3642	Fig. 4d)
$E_{Overall}$	0.357	1.28	–	–	0.3513	Fig. 4b)
	–	–	0.293	0.81	0.3241	Fig. 4d)

Fig. 4 shows the analysis of experimental data (from experiments performed as part of this study and from literature [18,23–33]) on the basis of the semi-empirical Gibson and Ashby model and the percolation theory (see Appendix for more details about each individual model).

From Fig. 4a), the semi-emprirical Gibson and Ashby model matches the individual properties analysed (E, UTS, and El) well, with R^2 values above 0.97 (with the exception of the elongation to failure), as the model is used to obtain the empirical C^* and n^* parameters (Table 2). Although with greater uncertainty, this empirical model still gives a rough overall (E+UTS+El) estimation of the variation of the properties for a specific set of data related to an isotropic porous pure metal (Fig. 4a, thick dashed line). Nevertheless, the model cannot satisfactorily predict the general variation of a specific properties, like E, of isotropic porous pure metals as the precision is significantly affected by the type of material (i.e. Ti, Fe or Al) and type of internal physical structure (Fig. 4b). It is worth mentioning that E was selected for analysing the general variation of a specific property of different porous materials in Fig. 4b because more data are available in literature. Similar conclusions to those of the Gibson and Ashby model are drawn from the analysis of experimental data through the percolation theory. It is accurate if empirical parameters are determined for a single set of data related to a specific property (Fig. 4c). However, the percolation theory cannot accurately predict the overall behaviour of a specific material or of different materials with the same level of volume fraction of pores (Fig. 4d).

3.2. Structural-analytical models

Different structural-analytical models (see Appendix for more details about each individual model considered in this study) generally work well for one type of porous material but might not necessarily be accurate for all types of porous materials. This is true even though the material is described as 'porous' leading to erroneous predictions, potentially of several orders of magnitude [34]. It is therefore of interest to compare the prediction of common structural-analytical models among themselves.

Fig. 5 shows the prediction of the tensile properties of isotropic porous pure metals using the different structural-analytical models described in the Appendix. The variation of the relative property with the volume fraction of pores for each structural-analytical model without experimental data is presented in Fig. 5a) along with the assumed physical structure of the porous material (insets in Fig. 5a). It is worth mentioning that $\psi_f / \psi_s = 0.02$ as the structural-analytical models were derived from the estimation of the physical properties (e.g. thermal conductivity) of porous samples.

As expected from the results of the characterisation of the tensile behaviour (Fig. 3), the tensile properties decrease with the increase of the volume fraction of pores. However, contrary to the trend of the absolute values, Fig. 5 shows that in general porous Fe has higher relative tensile properties (e.g. UTS) at lower volume fraction of pores and lower relative tensile properties at higher

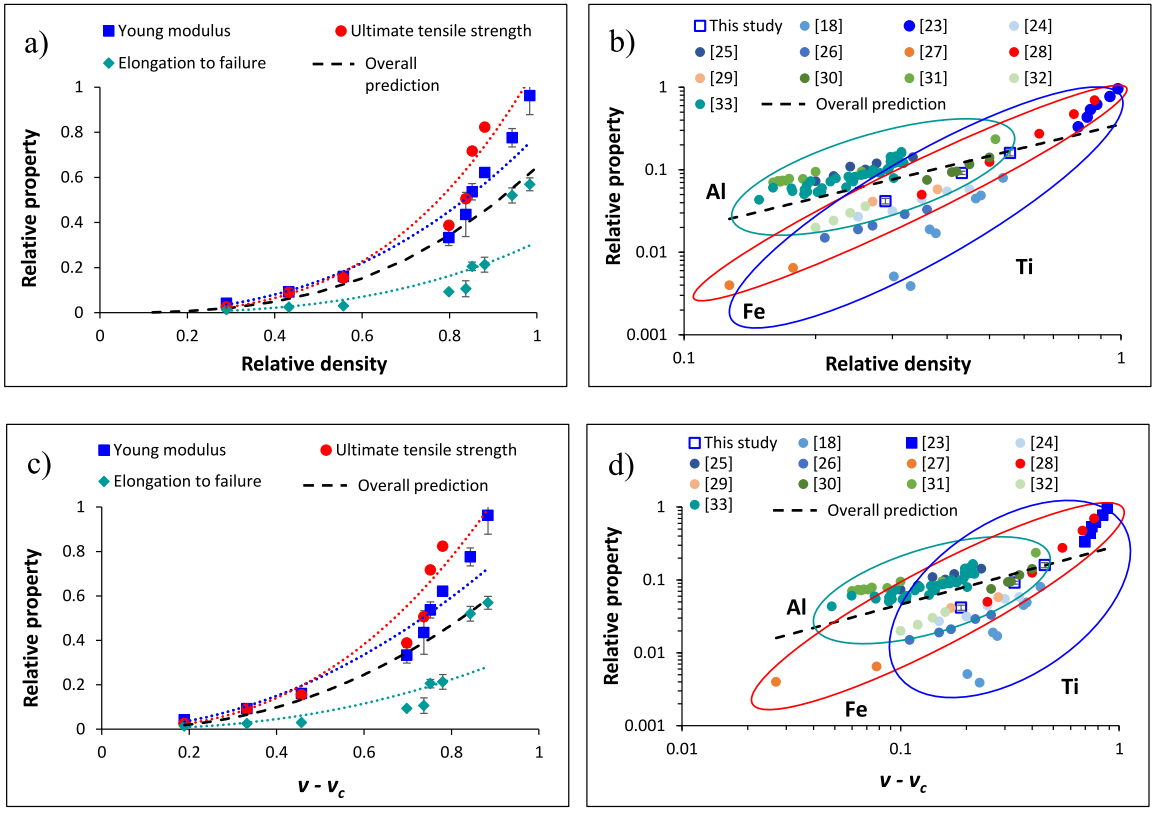

Fig. 4. Results of the analysis of the tensile properties of isotropic porous pure metals by means of empirical models: a) properties of porous Ti via the Gibson and Ashby model, b) E of porous Ti, Fe and Al [18,23–33] via the Gibson and Ashby model, c) properties of porous Ti via the percolation theory, d) E of porous Ti, Fe and Al [18,23–33] via the percolation theory.

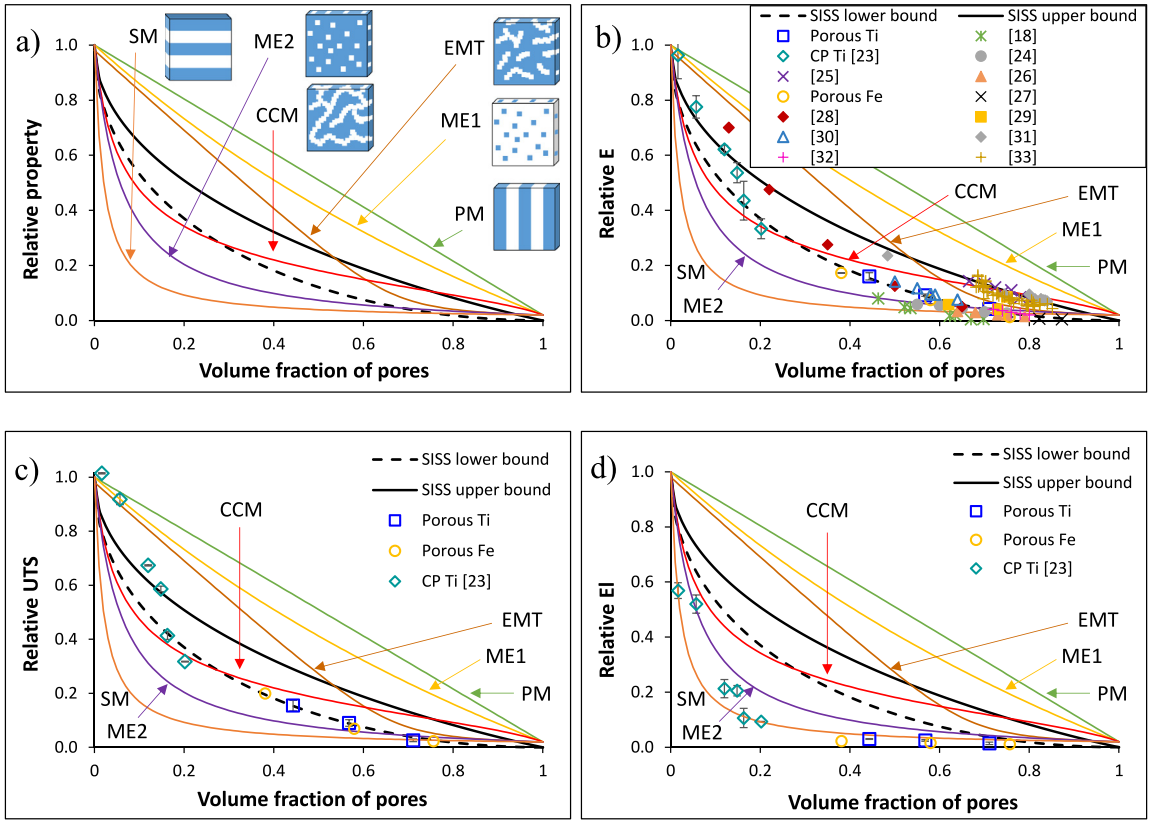

Fig. 5. Results of the analysis of the tensile properties of isotropic porous pure metals by means of different structural-analytical models: a) the models, b) E, c) UTS, and d) El. Note: PM (Parallel Model), ME1 (Maxwell-Eucken 1), EMT (Effective Medium Theory), CCM (Co-Continuous Model), ME2 (Maxwell-Eucken 2), and SM (Series Model) with $\psi_f/\psi_s = 0.02$.

volume fraction of pores. Furthermore, the comparison of the predictions of the structural-analytical models shows that, with the exception of the PM and ME1 (Maxwell-Eucken 1) models, most of the structural-analytical models will give a prediction in the range of the actual value of the Young modulus at high volume fraction of pores ($\geq$ 0.7). However, the SM and ME2 (Maxwell-Eucken 2) models tend to underestimate and the PM, ME1, EMT and co-continuous (CCM) models tend to significantly overestimate the value of the property under prediction. These trends are further exacerbated for lower volume fractions of pores. It is worth mentioning that, for plotting the curves of structural-analytical model predictions shown in Fig. 5, the mechanical properties of commercially pure (CP) Ti (isotropic properties: E = 110 GPa, UTS = 445–550 MPa, and El = 15–18% [35]) and those of pure Fe (isotropic properties: E = 200 GPa, UTS = 250 MPa, and El = 50% [36]) were used to calculate the relative values presented in Fig. 5.

Considering the whole range of volume fraction of pores, the symmetric and interconnected skeleton structural (SISS) model has the best overall fit and the highest accuracy for the prediction of E (Fig. 5b, mean square error of 2.2% and 3.0% for the lower and upper bound, respectively) and UTS (Fig. 5c, mean square error of 6.4% and 5.8% for the lower and upper bound, respectively) of porous metals. However, other structural-analytical models seem to be able to better predict the elongation to failure. Specifically, the SM model has the best overall fit, although perhaps not sufficiently accurate for prediction purposes. Because of these findings, a more in-depth analysis of the data presented in Fig. 5 was performed using the SISS model.

3.3. Analysis and validation of the prediction of the SISS model

The analysis of the tensile behaviour of the isotropic porous pure metals via the SISS model (Fig. 5) confirms that the SISS model [37] is able to effectively predict E and UTS of porous materials (Fig. 6b), at least in the range of volume fraction of pores analysed (0.38–0.75). Interestingly, the actual values of the tensile properties sit at the lower bound of the SISS model, which corresponds to hollow struts (v_h) with internal volume fraction of pores (i.e. fluid phase in the original work) equal to the external volume fraction of pores (i.e. $v_h = v_f/2$, where v_f is the volumetric fraction of pores). The isotropic porous pure metals are, however, primarily composed of solid interconnected struts (Fig. 2). This is due to the fact that, in contrast to other physical properties which rely on the transfer of particles (phonons and electrons, respectively, for thermal conductivity and electrical resistivity), the mechanical properties in general and the tensile behaviour in particular are not only dependent on the volume fraction of pores but they are also significantly affected by the structural features of the porous phase. In particular, the size (especially the maximum size) of the pores, the shape, and the actual distribution (location and distance between pores) are all important parameters as they determine localised stress concentration [38]. Monotonic failure of isotropic porous pure metals happens at *loci* where a defect of considerable size is withstanding a significantly higher load than the actual applied load (due to its size and morphology, and thus specific stress concentration factor), and where initiated cracks have a preferential crack growth path along closely spaced pores [39]. Among the tensile properties, ductility (and thus El) is the one most significantly influenced by the specific structural features of the pores which could explain why the SISS model significantly overestimates the value of the elongation to failure.

The validation of the prediction of the SISS model with data about porous Ti [18,23–26], porous Fe [27–29], and porous Al [30–33] (isotropic properties: E = 70 GPa, UTS = 60 MPa, and elongation to failure = 45% [40]) materials presented in Fig. 6 indicates that the SISS model can mathematically predict the Young modulus of isotropic porous pure metals and successfully discern between open cell and closed cell materials. Specifically, for volume fractions of pores above 0.4 it is found that foams with open cellular structure [18,23,24,26,30,32] are sitting at the lower bound of the SISS model whereas open cellular foams with closed cell substructures [25,27–29,31,33] are found at the upper bound. As the volume fraction of pores reduces below 0.4 down to 0.15, the experimental data transition from the lower bound to the upper bound of the model and therefore the model underestimates E.

The comprehensive analysis of Fig. 6 also confirms that the prediction of the UTS via the SISS model is accurate for volume fractions of pores down to 0.4 (data sitting at the lower bound), a transition from the lower to the upper bound occurs between 0.4 and 0.15, and the model underestimates the UTS for lower volume fraction of pores. The transition of the experimental data from the SISS lower bound to the SISS upper bound with the reduction of the volume fraction of pores is related to the transformation of the porous material from having internal interconnected porosity to having internal isolated porosity. It is worth mentioning that internal isolated porosity does not necessarily mean that the material is composed of isolated closed pores typical of materials sintered above 94% of their relative density [41]. The material is rather composed of pores that do not form a continuous network as their volume fraction is below the percolation threshold. Moreover, significant deviations are found also in the properties (i.e. E and UTS) in the 0–0.15 volume fraction of pores range. Regarding the elongation to failure (Fig. 6c), the SISS model always overestimates the ductility of the porous materials, even when the structure is only composed of closed pores (i.e. volume fraction of pores $\leq$ 0.05), not being able to account for the stress concentration factor of the residual pores.

4. Derivation of new combinatorial structural-analytical models for the estimation of the tensile behaviour of isotropic porous pure metals

Among the available structural-analytical models, the SISS model is currently the best to predict the tensile behaviour of isotropic porous pure metals. However, the model is only accurate in the 0.4–1.0 volume fraction of pores range and cannot satisfactorily predict the elongation to failure as it tends to overestimate it, even at high volume fraction of pores (Fig. 6c). The difference in performance between the prediction of E and UTS with respect to El rests on the susceptibility to crack formation/propagation and the ability to withstand damage.

Brailsford and Major [42] proposed a procedure to mathematically derive the EMT model by using the ME model for a material with two dispersed and one continuous phases. The same approach was taken by Wang et al. [19] to develop the CCM model assuming two continuous and one dispersed phases. The dispersed phase can then be eliminated assuming that its volume fraction is zero and each of its specific properties is the average of the two continuous phases. Mathematically this is express as Eq. (1):

$$v_1 \frac{(\psi_1 - \psi_{sample})(2\psi_1 + \psi_{sample})}{\psi_1} + v_2 \frac{(\psi_2 - \psi_{sample})(2\psi_2 + \psi_{sample})}{\psi_2} = 0 \quad (1)$$

Eq. (1) can be generalised for materials with N co-continuous phases as Eq. (2):

$$\sum_{i=1}^{N} v_i \frac{(\psi_i - \psi_{sample})(2\psi_i + \psi_{sample})}{\psi_i} = 0 \quad (2)$$

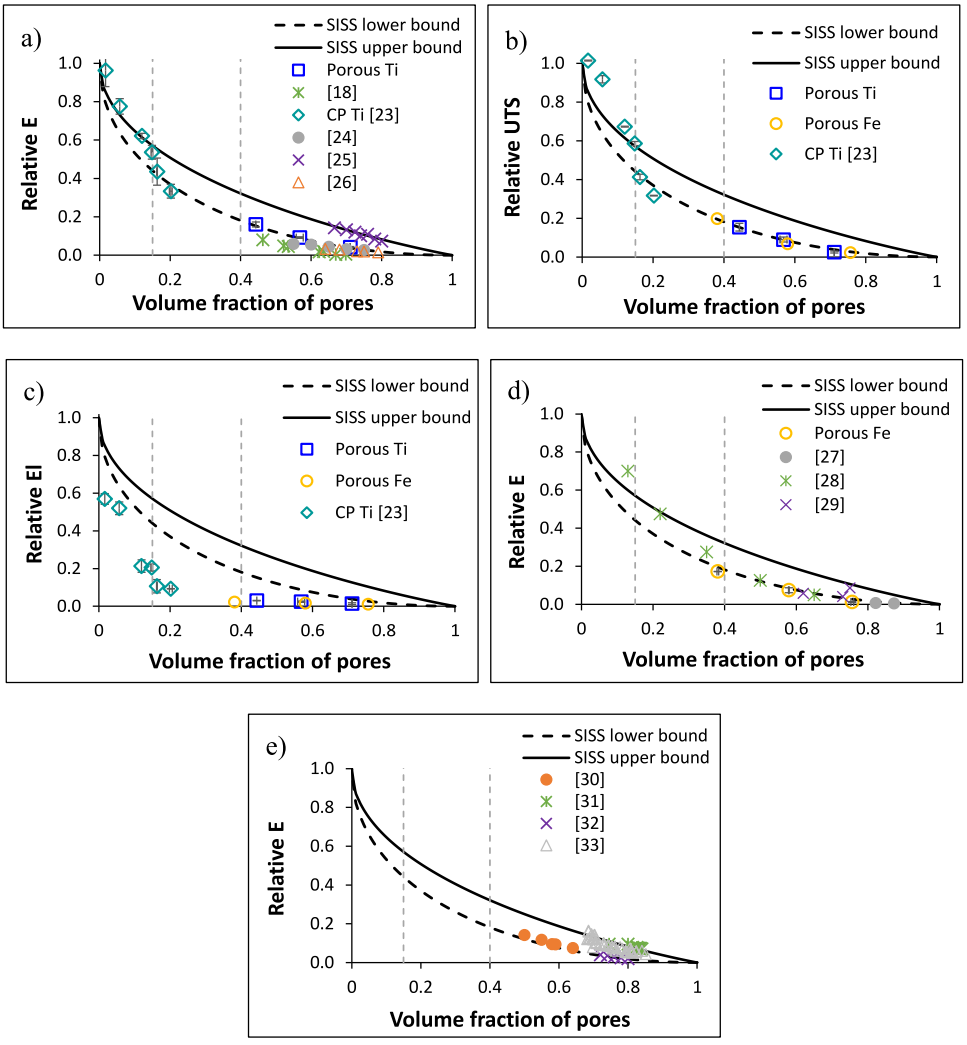

Fig. 6. Results of the validation of the prediction of the tensile behaviour via the SISS model: a) E of pure Ti [18,23–26], b) UTS, c) El, d) E of pure Fe [27–29], and d) E of pure Al [30–33]. Note: SISS lower and upper bounds for $\psi_f/\psi_s = 0$ (see Eq. (A12)).

Eq. (2) can then be rewritten as Eq. (3) by using the PM and SM models into the CCM model:

$$\psi_{sample} = \frac{\psi_{SM}}{2}\left(\sqrt{1+\frac{8\psi_{PM}}{\psi_{SM}}}-1\right) \tag{3}$$

where:

$$\psi_{SM} = \frac{1}{\sum_{i=1}^{N} v_i/\psi_i} \tag{4}$$

$$\psi_{PM} = \sum_{i=1}^{N} v_i\psi_i \tag{5}$$

The work of Brailsford and Major [42] reported a general equation for multi-component materials that can mathematically be used to derive the standard structural-analytical models reported in the Appendix (i.e. PM, ME1, EMT, ME2, and SM). New models are then generally created via combining different structural-analytical models using empirical weighting such as the harmonic weighting proposed by Krischer [43]:

$$\psi = \frac{1}{\frac{v}{\psi_{SM}} + \frac{(1-v)}{\psi_{PM}}} \tag{6}$$

From a more rigorous mathematical point of view, the complex physical structure assumed in Kirscher's approach can be approximated through assuming a mixture of several simpler structures. Making appropriate assumptions, this approach can then be used to derive binary-structure models by summing two models such as ME2+EMT as proposed by Wang et al. [44], where the associated physical structure is shown in Fig. 7a):

$$\begin{aligned}\psi_{sample} &= \frac{\psi_2 v_2\phi_{21} + \psi_1 v_1\phi_{11}\frac{3\psi_2}{2\psi_2+\psi_1}}{v_2\phi_{21} + v_1\phi_{11}\frac{3\psi_2}{2\psi_2+\psi_1}} \\ &= \frac{\psi_1 v_1\phi_{12}\frac{3\psi_{sample}}{2\psi_{sample}+\psi_1} + \psi_2 v_2\phi_{22}\frac{3\psi_{sample}}{2\psi_{sample}+\psi_2}}{v_1\phi_{12}\frac{3\psi_{sample}}{2\psi_{sample}+\psi_1} + v_2\phi_{22}\frac{3\psi_{sample}}{2\psi_{sample}+\psi_2}}\end{aligned} \tag{7}$$

However, this rigorous approach can easily lead to structural-analytical models that do not have an explicit form (such as in the case of the ME1+EMT and the ME2+EMT models [44]) where numerical iteration is required for solution. From a practical point of view, Eq. (3) (specific for the CCM model) combines the prediction of the SM (i.e. perpendicular layers of two alternating phases) and PM (i.e. parallel layers of two alternating phases) models to create a physical structure (co-continuous, Fig. 7b) different from the ones typical of the standard structural-analytical models (Fig. 5a). Following the same principle, several combinatorial physical structures can be obtained using the derived general form of the com-

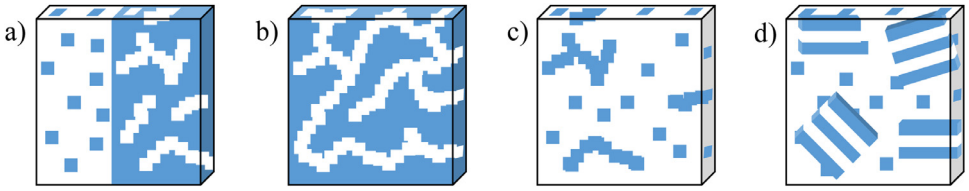

Fig. 7. Schematic representation of the physical structure of two-component materials derived from two fundamental structural-analytical models: a) ME2+EMT (Eq. (7)), b) PM combined with SM (viz. CCM model, Eq. (3)), c) combinatorial {ME2, EMT} model (Eq. (8)), and d) combinatorial {ME2, SM} model (Eq. (8)).

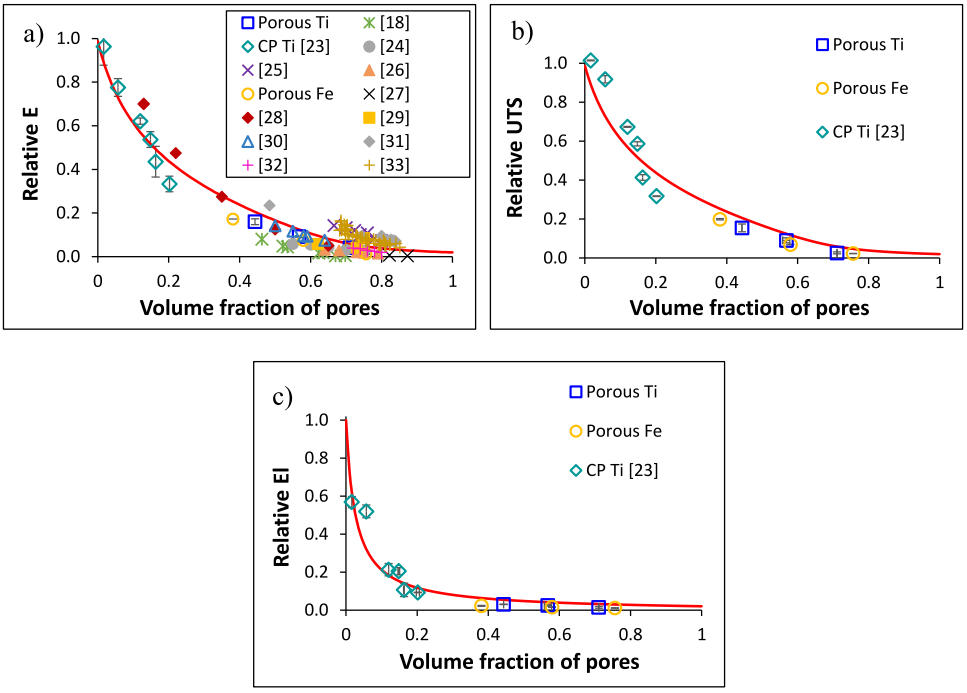

Fig. 8. Results of the analysis of the tensile properties of isotropic porous pure metals by means of derived combinatorial structural-analytical models ($\psi_f/\psi_s = 0.02$): a) E ({ME2, EMT} model), b) UTS ({ME2, EMT} model), and c) El ({ME2, SM} model).

bination of the structural-analytical models (Eq. (8)):

$$\psi_{sample} = \frac{\psi_{AM1}}{2}\left(\sqrt{1+\frac{8\psi_{AM2}}{\psi_{AM1}}}-1\right) \quad (8)$$

The data of the experiments of this study as well as those available in literature [18,23–33] were therefore analysed with several combinations of two structural-analytical models where the predicted behaviour was obtained via Eq. (8). The results of this analysis are summarised in Fig. 8 which presents the best prediction of the overall behaviour (regardless of the type of isotropic porous pure metal or internal structure) of each property (viz. E, UTS and El). Specifically, the combinatorial {ME2, EMT} and {ME2, S} structural-analytical models are the best to predict the overall E (mean square error of 1.8%) and UTS (mean square error of 2.2%) and El (mean square error of 0.5%) behaviours, respectively, over the whole range of volume fraction of pores. This is in agreement with the analysis of the data through the SISS model and strengthens the hypothesis that the toughness and ductility of the materials are much more affected by the characteristics of the pores.

Consequently, a unified model cannot be used to predict every individual tensile properties of isotropic porous pure metals but E and UTS can simultaneously be predicted through the combinatorial {ME2, EMT} model and El can be estimated via the combinatorial {ME2, SM} model. The associated physical structure of these two new combinatorial models are illustrated in Fig. 7. Both physical structures are predominantly based on the dispersion of one phase into another continuous phase (viz. {ME2}) but locally, within the continuous phase, there are stochastically distributed clusters of different dispersed phases (i.e. {EMT} or {SM}, Fig. 7c) or Fig. 7d)), respectively. The difference is related to the influence of the features of these clusters on the tensile behaviour of the porous materials where the SM model (i.e. second phase loaded perpendicularly to the direction of the applied tensile stress) is able to better take into account the effect of different stress concentration factors that the different type of pores have on the toughness and the ability to withstand damage before failure.

The derived combinatorial structural-analytical models are therefore useful tools to be able to rapidly and accurately predict the mechanical behaviour of isotropic porous pure metals. Optimisation of the properties of porous biomedical structural prostheses for the replacement of failed bones, of automotive devices able to absorb impact energy during crashes, and of porous insulating panels with reduce weight could be performed via the application of the derived combinatorial structural-analytical models discussed. Other potential use of isotropic porous pure metals where the estimation of their mechanical behaviour is crucial can be found in the review article by Evans et al. [45]. Suppose a porous metallic filter with 50% volume fraction of pores needs to be manufactured out of CP Ti grade 3. The derived combinatorial structural-analytical models of Fig. 8 shows that the filter will have E = 18.3 GPa ($0.167^{*}E_{Bulk\ Ti}$), UTS = 75 MPa ($0.167^{*}UTS_{Bulk\ Ti}$), and El = 0.84% ($0.047^{*}El_{Bulk\ Ti}$).

5. Conclusions

Empirical and structural-analytical models were applied to analyse the mechanical behaviour of isotropic porous pure metals both from purposely made samples and from data available in the literature. In general, semi-empirical models are very accurate for the prediction of the variation of a specific property of a particular material since experimental data are used to obtain the required empirical constants from that specific set of data. Consequently, empirical models cannot intrinsically predict the general behaviour of porous materials as shown by the analysis of different isotropic porous pure metals with different internal structures. Structural-analytical models, which have not received widespread use for the prediction of the mechanical behaviour, can give a more accurate estimation of the mechanical behaviour of porous materials. However, that is generally limited to a specific range of volume fraction of pores. Among the structural-analytical models analysed, the symmetric and interconnected skeleton structural (SISS) model gives the best prediction of the Young modulus and of the ultimate tensile strength (but always significantly overestimates the elongation to failure) over a reasonable range of volume fraction of pores (viz. 0.4–1.0). The new combinatorial structural-analytical models derived in this work are physically based, rapid, non-computing intensive models able to comprehensively and accurately predict the Young modulus plus ultimate tensile strength and the elongation to failure, respectively, across the whole volume fraction of pores even when the microstructure is unknown.

Data availability

All metadata pertaining to this work will be made available on request.

Declaration of Competing Interest

The authors declare no conflict of interest.

Acknowledgements

The financial support from MBIE (New Zealand Ministry of Business, Innovation and Employment) through the TiTeNZ project (UOWX1402 research contract) is sincerely acknowledged. LB would like to thank Dr. Mingtu Jia and Mr Jayden Monaghan for their technical contributions.

Appendix – Empirical and structural-analytical models

Different semi-empirical models are available but empirical constants need to be determined from experiments. Two of the most common empirical models were considered in this work and they are the Gibson and Ashby model and the percolation theory (A.1 and A.2, respectively). Several structural-analytical models are also available for the prediction of equivalent thermophysical properties where each model is based on an assumed physical structure (A.3-A.9). It is worth specifying that, although each structural-analytical model can mathematically predict the value of relative properties over the whole range of volume fraction of pores (i.e. from pure air, $v_f = 1$, to a completely solid material, $v_f = 0$), this does not necessarily correspond to a real physical situation. For example, the CCM model does not have physical meaning for volume fractions close to 0 or 1 as, respectively, the assumption of the co-continuity of the two phases cannot be met.

A.1. Gibson and Ashby model

The Gibson and Ashby model is based on micromechanical models based on dimensional arguments giving the dependence of the properties on the relative density (which is considered the single most important microstructural feature affecting the mechanical properties):

$$\frac{\psi_{sample}}{\psi_s} = C^* \left(\frac{\rho_{sample}}{\rho_s} \right)^{n^*} \tag{A1}$$

A.2. Percolation theory

The percolation theory is used in materials science to explain the drastic change in properties when a critical concentration (v_c) is reached. The theory relates the geometry and connectivity of randomly distributed clusters, which grow and eventually become interconnected resulting in the nonlinear scaling of properties. For microstructurally homogeneous materials is [46]:

$$\psi_{sample} = k(v - v_c)^t \tag{A2}$$

From the classical percolation theory, $v_c = 0.16$ and $t = 1.6$ for a perfectly stochastic 3D distribution of two components of a multimaterial (i.e. pores for porous materials) [47].

A.3. Parallel model (PM)

The parallel model is based on the assumption that the physical structure of the sample is composed of alternating layers of the two phases with parallel orientation to the axis of interest (e.g. heat flow direction):

$$\psi_{samples} = v_1 \psi_1 + v_2 \psi_2 \tag{A3}$$

A.4. Maxwell-Eucken 1 (ME1)

The Maxwell-Eucken 1 model is based on the assumption that the physical structure of the sample is composed of a dispersion of small spheres within a continuous matrix of a different component where ψ_1 is the continuous phase and ψ_2 is the dispersed phase:

$$\psi_{sample} = \frac{\psi_1 v_1 + \psi_2 v_2 \, \frac{3\psi_1}{2\psi_1 + \psi_2}}{v_1 + v_2 \, \frac{3\psi_1}{2\psi_1 + \psi_2}} \tag{A4}$$

A.5. Effective medium theory (EMT)

The effective medium theory is based on the assumption that the physical structure of the sample is composed of a completely stochastic distribution of the two phases:

$$(1 - v_2) \frac{\psi_1 - \psi_{sample}}{\psi_1 + 2\psi_{sample}} + v_2 \frac{\psi_2 - \psi_{sample}}{\psi_2 + 2\psi_{sample}} = 0 \tag{A5}$$

The value of ψ_{sample} can be derived from Eq. (A5) as:

$$\psi_{sample} = \frac{1}{4} \left\{ (3v_2 - 1)\psi_2 + (3v_1 - 1)\psi_1 + \sqrt{[(3v_2 - 1)\psi_2 + (3v_1 - 1)\psi_1]^2 + 8\psi_1\psi_2} \right\} \tag{A6}$$

A.6. Co-Continuous Model (CCM)

The co-continuous model is based on the assumption that the physical structure of the sample is composed of two co-continuous phases and derives from the combination of the PM and SM models (see Eq. (3)).

A.7. Maxwell-Eucken 2 (ME2)

The Maxwell-Eucken 2 model is based on the assumption that the physical structure of the sample is composed of a dispersion of small spheres within a continuous matrix of a different component where ψ_1 is the dispersed phase and ψ_2 is the continuous phase:

$$\psi_{sample} = \frac{\psi_2 v_2 + \psi_1 v_1 \frac{3\psi_2}{2\psi_2+\psi_1}}{v_2 + v_1 \frac{3\psi_2}{2\psi_2+\psi_1}} \tag{A7}$$

A.8. Series model (SM)

The series model is based on the assumption that the physical structure of the sample is composed of alternating layers of the two phases with perpendicular orientation to the axis of interest (e.g. heat flow direction).

$$\psi_{sample} = \frac{1}{\frac{v_1}{\psi_1} + \frac{v_2}{\psi_2}} \tag{A8}$$

A.9. Symmetric and interconnected skeleton structural (SISS) model

The symmetric and interconnected skeleton structural (SISS) model was proposed by Wang et al. [37], who demonstrated that the SISS model can effectively predict the physical properties of porous materials for the entire volume fraction of pores. This structural-analytical model, which can predict all the mathematically equivalent physical properties, is based on the observation that porous materials have a spatial symmetry in all three dimensions, specifically a common symmetric and interconnected strut structure. Therefore, the SISS model is built on assuming the struts of the physical structure to be hollow or solid, which respectively represents the lower and upper bound of the prediction, surrounded by pores (i.e. fluid phase). It is worth mentioning that the lower bound is obtained when the void fraction within the strut is the same as the void fraction outside the strut. The physical property of interest (e.g. thermal conductivity) needs then to be calculated for the 6 different prismatic structures that make up the unit cell of the model through a series of 18 equations (3 per prism) and finally combined in the PM model. However, if the value of the property of the solid phase (ψ_s) is significantly larger than that of the fluid phase (ψ_f), meaning that $\psi_f/\psi_s \approx 0$, the model is reduced to Eq. (A9) [37]:

$$\frac{\psi_{sample}}{\psi_s} = (a-b)^2 \tag{A9}$$

where:

$$a = 0.5 - cos\left[\frac{\pi + arccos\,(1 - 2v_s - 2v_h)}{3}\right] \tag{A10}$$

$$b = 0.5 - cos\left[\frac{\pi + arccos\,(1 - 2v_h)}{3}\right] \tag{A11}$$

In Eqs. (A9), (A10) and (A11), v_s and v_h are, respectively, the volume fraction of the solid phase and of the hollow struts phase and a and b are, respectively, the length of the outer and inner cross-sections of the struts forming the common 3D symmetric and interconnected microstructure. It is worth noticing that when $b = 0$ the structure is composed only of solid struts and therefore only v_s is needed to obtain the desired property as Eq. (A9) will transform into:

$$\frac{\psi_{sample}}{\psi_s} = \left\{0.5 - cos\left[\frac{\pi + arccos\,(1 - 2v_s)}{3}\right]\right\}^2 \tag{A12}$$

References

[1] F. Barthelat, Architectured materials in engineering and biology: fabrication, structure, mechanics and performance, Int. Mater. Rev. 60 (2015) 413–430.
[2] L.J. Gibson, Annual review of materials science, Ann. Rev. (2000) 191–227.
[3] J. Banhart, H.W. Seeliger, Aluminium foam sandwich panels: manufacture, metallurgy and applications, Adv. Eng. Mater. 10 (2008) 793–802.
[4] K. Grilec, G. Marić, S. Jakovljević, A study on energy absorption of aluminium foam, BHM Berg- und Hüttenmännische Monatshefte 155 (2010) 231–234.
[5] A. Bhattacharya, R.L. Mahajan, Finned metal foam heat sinks for electronics cooling in forced convection, J. Electron. Packag. 124 (2002) 155–163.
[6] A. Oriňák, R. Oriňáková, Z.O. Králová, A.M. Turoňová, M. Kupková, M. Hrubovčáková, J. Radoňák, R. Džunda, Sintered metallic foams for biodegradable bone replacement materials, J. Porous Mater. 21 (2014) 131–140.
[7] L. Bolzoni, M. Nowak, N.Hari Babu, Assessment of the influence of Al-2Nb-2B master alloy on the grain refinement and properties of LM6 (A413) alloy, Mater. Sci. Eng.: A 628 (2015) 230–237.
[8] M. Thieme, K.P. Wieters, F. Bergner, D. Scharnweber, H. Worch, J. Ndop, T.J. Kim, W. Grill, Titanium powder sintering for preparation of a porous functionally graded material destined for orthopaedic implants, J. Mater. Sci. Mater. Med. 12 (2001) 225–231.
[9] V. Mironov, A. Tatarinov, V. Lapkovsky, Consolidation of metallic hollow spheres by electric sintering, IOP Conf. Ser.: Mater. Sci. Eng. 218 (2017) 012009.
[10] E.E. Aşik, Â. Bor, Fatigue behavior of Ti-6A-4V foams processed by magnesium space holder technique, Mater. Sci. Eng.: A 621 (2015) 157–165.
[11] N.G. Davis, J. Teisen, C. Schuh, D.C. Dunand, Solid-state foaming of titanium by superplastic expansion of argon-filled pores, J. Mater. Res. 16 (2011) 1508–1519.
[12] I.-.H. Oh, N. Nomura, S. Hanada, Microstructures and mechanical properties of porous titnaium compacts prepared by powder sintering, Mater. Trans. JIM 43 (2002) 443–446.
[13] L. Bolzoni, E.M. Ruiz-Navas, E. Gordo, Investigation of the factors influencing the tensile behaviour of PM Ti-3Al-2.5V alloy, Mater. Sci. Eng. A 609 (2014) 266–272.
[14] M.M. Shbeh, R. Goodall, Open celled porous titanium, Adv. Eng. Mater. 19 (2017) 1600664.
[15] R. Landauer, The electrical resistance of binary metallic mixtures, J. Appl. Phys. 23 (1952) 779–784.
[16] A. Bhattacharya, V.V. Calmidi, R.L. Mahajan, Thermophysical properties of high porosity metal foams, Int. J. Heat Mass Transfer 45 (2002) 1017–1031.
[17] L.J. Gibson, M.F. Ashby, Cellular Solids, Structures, and Properties, 2nd ed., Cambridge, 1997.
[18] Z. Esen, Ş. Bor, Processing of titanium foams using magnesium spacer particles, Scr. Mater. 56 (2007) 341–344.
[19] J. Wang, J.K. Carson, M.F. North, D.J. Cleland, A new structural model of effective thermal conductivity for heterogeneous materials with co-continuous phases, Int. J. Heat Mass Transfer 51 (2008) 2389–2397.
[20] S. Torquato, Random Heterogeneous Materials, Springer Verlag, New york, 2002.
[21] S. Raynova, M.A. Imam, F. Yang, L. Bolzoni, Hybrid microwave sintering of blended elemental Ti alloys, J. Manuf. Processes 39 (2019) 52–57.
[22] L. Bolzoni, F. Yang, Development of Cu-bearing powder metallurgy Ti alloys for biomedical applications, J. Mech. Behav. Biomed. Mater. 97 (2019) 41–48.
[23] S. Raynova, Y. Collas, F. Yang, L. Bolzoni, Advancement in the pressureless sintering of CP titanium using high-frequency induction heating, Metall. Mater. Trans. A 50 (2019) 4732–4742.
[24] W. Niu, C. Bai, G. Qiu, Q. Wang, Processing and properties of porous titanium using space holder technique, Mater. Sci. Eng.: A 506 (2009) 148–151.
[25] N. Jha, D.P. Mondal, J. Dutta M., A. Badkul, A.K. Jha, A.K. Khare, Highly porous open cell Ti-foam using NaCl as temporary space holder through powder metallurgy route, Mater. Des. 47 (2013) 810–819.
[26] A. Mansourighasri, N. Muhamad, A.B. Sulong, Processing titanium foams using tapioca starch as a space holder, J. Mater. Process. Technol. 212 (2012) 83–89.
[27] B. Wegener, A. Sichler, S. Milz, C. Sprecher, K. Pieper, W. Hermanns, V. Jansson, B. Nies, B. Kieback, P.E. Müller, V. Wegener, P. Quadbeck, Development of a novel biodegradable porous iron-based implant for bone replacement, Sci. Rep. 10 (2020) 9141.
[28] M. Vesenjak, A. Kovačič, M. Tane, M. Borovinšek, H. Nakajima, Z. Ren, Compressive properties of lotus-type porous iron, Comput. Mater. Sci. 65 (2012) 37–43.
[29] R. Alavi, A. Trenggono, S. Champagne, H. Hermawan, Investigation on mechanical behavior of biodegradable iron foams under different compression test conditions, Metals 7 (2017).
[30] M. Wicklein, K. Thoma, Numerical investigations of the elastic and plastic behaviour of an open-cell aluminium foam, Mater. Sci. Eng.: A 397 (2005) 391–399.
[31] J. Kováčik, L. Marsavina, E. Linul, Poisson's ratio of closed-cell aluminium foams, Materials 11 (2018).
[32] C. San Marchi, A. Mortensen, Deformation of open-cell aluminum foam, Acta Mater. 49 (2001) 3959–3969.
[33] I. Sevostianov, J. Kováčik, F. Simančík, Elastic and Electric properties of closed–cell aluminum foams: cross-property connection, Materials Science and Engineering: A 420 (2006) 87–99.
[34] J.K. Carson, S.J. Lovatt, D.J. Tanner, A.C. Cleland, Thermal conductivity bounds for isotropic, porous materials, Int. J. Heat Mass Transfer 48 (2005) 2150–2158.

[35] R. Boyer, G. Welsch, E.W. Collings, in: A. International (Ed.), Ohio, USA, 1998.
[36] E. Lucon, K. Abiko, M. Lambrecht, B. Rehmer, in: Tensile Properties of Commercially Pure, High-Purity and Ultra-High-Purity Iron: Results of an International Round-Robin, National Institute of Standards and Technology, 2015, pp. 1–32. NIST Technical Note 1879.
[37] J.F. Wang, J.K. Carson, J. Willix, M.F. North, D.J. Cleland, A symmetric and interconnected skeleton structural (SISS) model for predicting thermal and electrical conductivity and Young's modulus of porous foams, Acta Mater. 56 (2008) 5138–5146.
[38] A. Hadrboletz, B. Weiss, Fatigue behaviour of iron based sintered material: a review, Int. Mater. Rev. 42 (1997) 1–44.
[39] C. Romero, F. Yang, L. Bolzoni, Fatigue and fracture properties of Ti alloys from powder-based processes - a review, Int. J. Fatigue 117 (2018) 407–419.
[40] J.R. Davis, ASM Speciality Handbook: Aluminium and Aluminium Alloys, First printing ed., Ohio, USA, 1993.
[41] R.M. German, Sintering Theory and Practice, Wiley, New York, 1996.
[42] A.D. Brailsford, K.G. Major, The thermal conductivity of aggregates of several phases, Including Porous Mater. Br. J. Appl. Phys. 15 (1964) 313–319.
[43] O. Krischer, Die Wissenschaftlichen Grundlagen der Trocknungstechnik, The Scientific Fundamentals of Drying Technology, Berlin, 1963.
[44] J. Wang, J.K. Carson, M.F. North, D.J. Cleland, A new approach to modelling the effective thermal conductivity of heterogeneous materials, Int. J. Heat Mass Transfer 49 (2006) 3075–3083.
[45] A.G. Evans, J.W. Hutchinson, M.F. Ashby, Multifunctionality of cellular metal systems, Prog. Mater Sci. 43 (1998) 171–221.
[46] H. Du, X. Lin, H. Zheng, B. Qu, Y. Huang, D. Chu, Colossal permittivity in percolative ceramic/metal dielectric composites, J. Alloys Compd. 663 (2016) 848–861.
[47] L. Bolzoni, Structural electroactive cermets: dielectric and structural properties of conductive metallic reinforced piezoelectric ceramics, Crit. Rev. Solid State Mater. Sci. (2019) 1–44.